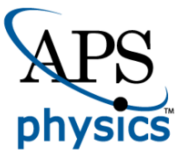

Strong coupling of a quantum dot molecule to a photonic crystal cavity

Patrick M. Vora, Allan S. Bracker, Samuel G. Carter, Mijin Kim, Chul Soo Kim, and Daniel Gammon

Phys. Rev. B **99**, 165420 — Published 15 April 2019

DOI: 10.1103/PhysRevB.99.165420

Strong coupling of a quantum dot molecule to a photonic crystal cavity

Patrick M. Vora[1,2,*], Allan S. Bracker[3], Samuel G. Carter[3], Mijin Kim[4], Chul Soo Kim[3], and Daniel Gammon[3]

[1] *Department of Physics and Astronomy, George Mason University, Fairfax, VA 22030, USA*
[2] *Quantum Materials Center, George Mason University, Fairfax, VA 22030, USA*
[3] *Naval Research Laboratory, Washington, DC 20375, USA*
[4] *Sotera Defense Solutions, Inc., Columbia, MD 21046, USA*
[*]Corresponding author: PMV, pvora@gmu.edu.

Quantum dot molecules have widely tunable exciton transition energies and transition strengths that can be controlled with an applied electric field. We use these properties to demonstrate *in situ* tuning of the vacuum Rabi splitting for a quantum dot molecule embedded in a photonic crystal cavity. Both components of the anisotropic exchange doublet have a component parallel to the cavity and are strongly coupled. This produces two QDM-cavity polaritons with properties dominated by the cavity and a third mixed-spin hybrid state with little cavity component and unusual polarization.

Semiconductor quantum dots (QDs) coupled to optical microcavities are a proven platform for exploring cavity quantum electrodynamics. Observations of strong coupling, single photon emission, non-classical light, and few-photon optical nonlinearities suggest promising applications for quantum photonics technologies [1]. To date, the field has focused on cavity-exciton interactions in single QDs. Considerable effort has been devoted to maximizing the light-matter interaction by matching the energy of the cavity resonance and the QD resonance. The most common energy tuning techniques are gas adsorption to vary the effective cavity size [2] or temperature to vary the semiconductor bandgap [3]. An electric field can also be used to shift QD exciton energies [4–7] although the tuning range is limited by the small QD dipole moments.

New capabilities are offered by quantum dot molecules (QDMs), which consist of two QDs separated by a tunnel barrier. The combination of carrier tunneling and electron-hole spatial separation produces a rich spectral structure [8–10] that has enabled nondestructive spin readout [11,12] extended spin lifetimes [13], cavity-stimulated Raman photon generation [14] and ultrafast pulse shaping [15]. Here, we take advantage of the wide energy tunability of QDMs to explore cavity quantum electrodynamics in the strong coupling regime for a neutral molecular exciton.

Excitons in a QDM can be spatially direct or indirect, with the electron-hole pair confined in one QD or separated between the QDs, respectively. Quantum tunneling between the QDs mixes the two types of excitons. In a plot of energy vs. electric field, tunneling manifests as an anticrossing with a smooth transition between direct and indirect exciton states [8,9]. Figure 1a shows QDM exciton levels as a function of the applied bias ($\propto$ field) in a diode heterostructure. The unmixed direct and indirect states are shown with dashed lines. Regions of the anticrossing with large slope have indirect exciton character, resulting in a large static dipole and a small optical transition dipole. As the slope decreases and the exciton becomes more direct, the electron-hole

separation decreases [9], and the static and transition dipoles evolve continuously to small and large, respectively.

The QDMs are embedded in a *n-i-n-i-p* GaAs membrane diode [16–18], which provides control of electric field and charging. The membrane is patterned into a photonic crystal containing L3 defect cavities. Further details of the device heterostructure and fabrication are provided in [19]. PL measurements were performed at 5 K with an 870 nm laser polarized orthogonal to the cavity mode. Polarization angles are referenced to the lowest-energy mode of the L3 defect cavity [20] and we deposit Xe to redshift the mode energy as needed [2]. For polarization-resolved measurements, PL was directed through an analyzer and half-wave-plate to a triple spectrometer with 15 μeV or 70 μeV resolution, depending on its configuration.

Fig. 1b shows the QDM PL spectrum as a function of diode bias near the neutral exciton (X^0) anticrossing, the energies of which have been modelled in Fig. 1a. Here the cavity mode has been shifted to the red by 8 meV. In this work, we will focus on the lower branch of the anticrossing (yellow & black dashed box), which is brighter due to carrier relaxation from the upper branch. Intense lines at other energies correspond to charged excitons (X^+, X^{2+}, X^-) and biexciton (XX^0), and are discussed briefly in [19]. Despite the overall complex appearance of Fig. 1b, the relevant physics addressed here is confined to the lower X^0 anticrossing feature and its spin fine structure.

Exciton spin fine structure makes a prominent contribution to the appearance of the cavity-modulated spectrum. This fine structure arises from electron-hole exchange [21], and is only present in the direct component of QDM excitons [22,23] where electron-hole spatial overlap is large. The fine structure is summarized in Fig. 1(c), with a small anisotropic exchange splitting (δ_1) between the bright excitons (X_1, X_2) and a larger splitting (δ_0) between bright and dark (normally forbidden) excitons. Although the spectrometer cannot fully resolve δ_1, the unresolved peaks have opposite linear polarization [21], and measuring them with a polarization filter as a function of angle [24] gives the splitting $\delta_1 \approx 20\mu$eV and the X_2 exciton state orientation as $\theta \approx 24°$ relative to the cavity polarization [Fig. 1(d)]. This measurement was carried out at a bias of 0.515 V where the exciton is predominantly direct.

We first examine cavity-exciton coupling in the bias-dependent PL spectra, where the direct and indirect excitonic character is tunable. These spectra are compared to a phenomenological Hamiltonian model, described in [19], that includes electron tunneling, electron-hole exchange, and cavity coupling. Fig. 2a shows the spectrum with the cavity mode tuned to an energy of 1294.27 meV, where the exciton anticrossing peak has a large slope and a moderate-sized component of indirect character. The wavefunction direct exciton coefficient where the cavity intersects is estimated at ~0.83 from the model. In this situation, the radiative emission rate is relatively small, and the vacuum Rabi splitting is not clearly resolved. As observed previously with a single QD [25], the dark exciton peak (X_d) is enhanced in intensity through cavity-induced mixing with the bright states. Mixing with the cavity also has a strong influence on the fine structure spitting. Above the cavity resonance, the two states derived from bright excitons X_1 and X_2 (labelled "B'' and "C'') have a splitting of ~50 μeV, which is considerably larger than δ_1 (~20 μeV). This effective spin splitting is larger, because it contains a small contribution of vacuum Rabi splitting. The fact that the splitting changes very little at energies above the cavity resonance (bias range 0.44V-0.48V) arises from the tradeoff between cavity detuning and direct

exciton character, which both increase toward higher energies but act in the opposite sense on the cavity-exciton interaction.

When the cavity is tuned to 1294.77 meV (Fig. 2b), it intersects where the exciton direct coefficient is somewhat larger (~0.92). The observed vacuum Rabi structure results from both fine structure components being strongly coupled to the cavity. The state labels used here distinguish between the coupled (*A*, *B*, *C*) and uncoupled states (X_1, X_2, cavity). The lower and upper polaritons are *A* and *C*, and an additional state *B* passes between them. Peak *B* evolves continuously from the upper fine structure component X_2 below the cavity resonance into the lower component X_1 above the cavity resonance. The polariton peaks *A* and *C* are broadened due to their large cavity component, while peak *B* remains narrow. At energies above the cavity resonance, where the direct exciton fraction is larger, the splitting between *B* and *C* is large compared to δ_1. In contrast, peaks *A* and *B* merge on the lower energy side, where the direct exciton fraction of peak *A* is smaller. We consider this structure in more detail in the context of Figs 3 and 4.

We note that the vacuum Rabi splitting in Fig. 1b is partly obscured by cavity emission that appears as a band over the entire bias range. These features do not appear in the modelled spectra on the right-hand side. This light is created by nearby charged excitons with their main features at other energies, including X^- (~1294 meV) and X^+ (~1293 meV), that non-resonantly feed the cavity. Although at any instant in time the QD exists in only one charge configuration, the configuration fluctuates during our time-integrated measurements over many seconds.

Fig. 2 highlights that a QDM provides two tunable parameters for light-matter coupling. One is the wide energy range spanned by indirect transitions, because of their large static dipoles. The second is the coupling strength, which is available near tunneling anticrossings where the direct exciton fraction varies continuously. Naturally, there is a tradeoff between these, since a large static dipole moment implies a large electron-hole separation and therefore a smaller transition dipole. A compromise can be achieved by adjusting the interdot barrier thickness. The tunability of coupling strength is summarized in Fig. 2c, which plots $2g$ against the direct exciton wavefunction coefficient obtained from the model. The coupling strength $2g$ (left axis) was obtained [26] from the measured vacuum Rabi splitting Δ by $2g = \sqrt{\Delta^2 + \frac{1}{4}(\Gamma_T - \kappa)^2}$, where Γ_T is the FWHM linewidth of X_1 measured at each bias and $\kappa = 200\,\mu eV$ is the FWHM cavity linewidth. The red line is a linear fit, which assumes that $2g$ is proportional to the transition dipole moment for the direct exciton component of the QDM exciton wavefunction [27]. In the simplest model, one expects the line to pass through the origin, but for unknown reasons the horizontal intercept is 0.55.

Fig. 3a shows the vacuum Rabi anticrossing measured in the alternative approach, where the cavity resonance is tuned through the fixed exciton transition using Xe gas. Here the bias is fixed at ~ 0.460 V, where the exciton has a large direct coefficient and strong coupling to the cavity. This structure can be compared to Figure 3c, which shows the modelled spectrum. Box ii in Figs 3a and 3b corresponds to a zero cavity-exciton detuning and shows the sharp middle peak *B* with broadened polariton peaks *A* and *C* to either side. At negative detuning, peaks *A*, *B*, and *C* evolve into the cavity mode, X_1, and X_2, respectively. At positive detuning they evolve into X_1, X_2, and

the cavity mode. We have fit the peaks in Fig. 3b with Lorentzians to more clearly show their positions and widths.

For both fine structure states to be strongly coupled, each must have a component of polarization parallel to the cavity. In the common situation where the fine structure states are aligned with the [110]-like crystal axes, only one state will be parallel to the cavity [25], which in our devices is also aligned to the crystal axes. However, a strong asymmetry in alloy composition or strain will misalign the fine structure axes from the crystal axes [24,28,29], leading to strong coupling of both states. This may be more likely to happen in self-assembled QDMs [30], where the individual QDs are mutually strained and not vertically aligned.

Near the anticrossing, peak *B* is a cavity-induced hybrid wavefunction of the two exciton spin states. Interestingly, the cavity itself is largely excluded from the wavefunction. This is evident from its sharp linewidth and confirmed by the model calculation where the peak *B* wavefunction contains only 0.4% cavity mode. In fact, the cavity contribution to *B* would be 0% if both excitons were polarized at 45° to the cavity mode. Here they are 114° and 24°, which mixes the excitons unequally and brings a small amount of polariton character into state *B*.

The hybrid spin-state nature of peak *B* leads to interesting polarization-dependent behavior as shown in Fig. 4. The PL spectrum at the anticrossing was measured for a series of polarizer angles (Fig. 4a) and fit with Lorentzians, with the resulting intensities plotted in Fig 4b. The purple arrows indicate the direction of the X_1 and X_2 polarization axes at their native angles of 114° and 24° when the cavity is detuned. The polariton peaks *A* and *C* are co-polarized with the cavity (blue points), while the hybrid state *B* has elliptical polarization (red points) and is aligned nearly along the native exciton axes. To understand these observations, the angle-dependence of the emission intensity of peak *B* is calculated from the projection of the transition dipole moment $\boldsymbol{p}_B$ onto the polarizer orientation, $I \propto |\boldsymbol{p}_B \cdot \hat{n}|^2$, where

$$\boldsymbol{p}_B = \langle X|\boldsymbol{r}|GS,0\rangle \;\propto\; \alpha_c e^{i\eta} N_c \hat{x} + i\alpha_1 \hat{u}_1 + \alpha_2 \hat{u}_2, \qquad (1)$$

and the unit vectors $\hat{x}$, $\hat{u}_1$, and $\hat{u}_2$ correspond to the cavity and exciton axes, respectively. The wavefunction coefficients for the eigenstates are determined from the Hamiltonian and are denoted α_c, α_1, and α_2 for the contributions from the cavity, X_1, and X_2 respectively, and we assume that the indirect exciton states have a negligible contribution because of their small transition dipole moment. N_c accounts for the cavity's faster emission rate relative to the QD and the phase factor $e^{i\eta}$ allows the cavity term to be complex. The data is well-fit with $N_c = 3.3$ and $\eta = 198^\circ$ for state *B*. The ellipticity and polarization angle are sensitive to these fit parameters, demonstrating the importance of cavity-induced mixing in state *B* despite its small value of α_c. For the polariton states *A* and *C*, which have large values of α_c, the polarization is dominated by the cavity.

We have investigated a QDM strongly-coupled to a photonic crystal cavity. This system provides additional degrees of freedom unavailable in cavity-coupled single QDs. Specifically, the tunable electron-hole separation for a QDM exciton changes both the static dipole and the optical transition dipole, thereby tuning both the transition energy and strength and providing control over the vacuum Rabi splitting. We find that both exciton fine structure components are strongly coupled, which may be more likely to happen in a QDM due to strain-induced asymmetry that misaligns the exciton polarization from the crystal axes. In this situation, two polariton states and

a cavity-induced spin hybrid state are formed. The emission polarization for all three states is strongly influenced by the cavity, despite one state having very little cavity admixture.

Acknowledgements

P.M.V. acknowledges support under NSF EAGER grant DMR-1748650 and the George Mason University Quantum Materials Center. This work was supported by the Office of Naval Research.

References

[1] P. Lodahl, S. Mahmoodian, and S. Stobbe, Rev. Mod. Phys. **87**, 347 (2015).

[2] S. Mosor, J. Hendrickson, B. C. Richards, J. Sweet, G. Khitrova, H. M. Gibbs, T. Yoshie, A. Scherer, O. B. Shchekin, and D. G. Deppe, Appl. Phys. Lett. **87**, 141105 (2005).

[3] A. Faraon, D. Englund, I. Fushman, J. Vuc□ković, N. Stoltz, and P. Petroff, Appl. Phys. Lett. **90**, 213110 (2007).

[4] A. Laucht, F. Hofbauer, N. Hauke, J. Angele, S. Stobbe, M. Kaniber, G. Böhm, P. Lodahl, M.-C. Amann, and J. J. Finley, New J. Phys. **11**, 023034 (2009).

[5] A. Laucht, J. M. Villas-Bôas, S. Stobbe, N. Hauke, F. Hofbauer, G. Böhm, P. Lodahl, M.-C. Amann, M. Kaniber, and J. J. Finley, Phys. Rev. B **82**, 075305 (2010).

[6] M. Rakher, N. Stoltz, L. Coldren, P. Petroff, and D. Bouwmeester, Phys. Rev. Lett. **102**, 097403 (2009).

[7] R. J. Warburton, C. Schäflein, D. Haft, F. Bickel, A. Lorke, K. Karrai, J. M. Garcia, W. Schoenfeld, and P. M. Petroff, Nature **405**, 926 (2000).

[8] E. A. Stinaff, M. Scheibner, A. S. Bracker, I. V Ponomarev, V. L. Korenev, M. E. Ware, M. F. Doty, T. L. Reinecke, and D. Gammon, Science (80-.). **311**, 636 (2006).

[9] M. Scheibner, A. Bracker, D. Kim, and D. Gammon, Solid State Commun. **149**, 1427 (2009).

[10] M. F. Doty, M. Scheibner, A. S. Bracker, I. V. Ponomarev, T. L. Reinecke, and D. Gammon, Phys. Rev. B **78**, 115316 (2008).

[11] D. Kim, S. Economou, Ş. Bădescu, M. Scheibner, A. Bracker, M. Bashkansky, T. Reinecke, and D. Gammon, Phys. Rev. Lett. **101**, 236804 (2008).

[12] A. N. Vamivakas, C.-Y. Lu, C. Matthiesen, Y. Zhao, S. Fält, A. Badolato, and M. Atatüre, Nature **467**, 297 (2010).

[13] K. M. Weiss, J. M. Elzerman, Y. L. Delley, J. Miguel-Sanchez, and A. Imamo□lu, Phys. Rev. Lett. **109**, 107401 (2012).

[14] P. M. Vora, A. S. Bracker, S. G. Carter, T. M. Sweeney, M. Kim, C. S. Kim, L. Yang, P. G. Brereton, S. E. Economou, and D. Gammon, Nat. Commun. **6**, 7665 (2015).

[15] B. C. Pursley, S. G. Carter, M. K. Yakes, A. S. Bracker, and D. Gammon, Nat. Commun. **9**, 115 (2018).

[16] M. C. Löbl, I. Söllner, A. Javadi, T. Pregnolato, R. Schott, L. Midolo, A. V. Kuhlmann, S. Stobbe, A. D. Wieck, P. Lodahl, A. Ludwig, and R. J. Warburton, Phys. Rev. B **96**, 165440 (2017).

[17] K. G. Lagoudakis, K. Fischer, T. Sarmiento, A. Majumdar, A. Rundquist, J. Lu, M. Bajcsy, and J. Vučković, New J. Phys. **15**, 113056 (2013).

[18] S. G. Carter, T. M. Sweeney, M. Kim, C. S. Kim, D. Solenov, S. E. Economou, T. L. Reinecke, L. Yang, A. S. Bracker, and D. Gammon, Nat. Photonics **7**, 329 (2013).

[19] See Supplemental Material at http://link.aps.org/supplemental/10.1103/PhysRevB.000.000000 for details on the sample structure, QDM PL spectra, and the phenomenological Hamiltonian.

[20] A. Kress, F. Hofbauer, N. Reinelt, M. Kaniber, M. Bichler, D. Schuh, G. Boehm, and J. J. Finley, in *Photonic Cryst. Mater. Devices III*, edited by A. Adibi, S.-Y. Lin, and A. Scherer (SPIE, 2005), p. 114.

[21] D. Gammon, E. S. Snow, B. V. Shanabrook, D. S. Katzer, and D. Park, Phys. Rev. Lett. **76**, 3005 (1996).

[22] M. Scheibner, M. F. Doty, I. V. Ponomarev, A. S. Bracker, E. A. Stinaff, V. L. Korenev, T. L. Reinecke, and D. Gammon, Phys. Rev. B **75**, 245318 (2007).

[23] M. Scheibner, I. V. Ponomarev, E. A. Stinaff, M. F. Doty, A. S. Bracker, C. S. Hellberg, T. L. Reinecke, and D. Gammon, Phys. Rev. Lett. **99**, 197402 (2007).

[24] J. D. Plumhof, V. Křápek, F. Ding, K. D. Jöns, R. Hafenbrak, P. Klenovský, A. Herklotz, K. Dörr, P. Michler, A. Rastelli, and O. G. Schmidt, Phys. Rev. B **83**, 121302 (2011).

[25] M. Winger, A. Badolato, K. J. Hennessy, E. L. Hu, and A. Imamo□lu, Phys. Rev. Lett. **101**, 1 (2008).

[26] M. Kaniber, A. Laucht, T. Hürlimann, M. Bichler, R. Meyer, M.-C. Amann, and J. J. Finley, Phys. Rev. B **77**, 073312 (2008).

[27] D. Englund, D. Fattal, E. Waks, G. Solomon, B. Zhang, T. Nakaoka, Y. Arakawa, Y. Yamamoto, and J. Vučković, Phys. Rev. Lett. **95**, 013904 (2005).

[28] S. Seidl, B. D. Gerardot, P. A. Dalgarno, K. Kowalik, A. W. Holleitner, P. M. Petroff, K. Karrai, and R. J. Warburton, Phys. E **40**, 2153 (2008).

[29] G. W. Bryant, M. Zieliński, N. Malkova, J. Sims, W. Jaskólski, and J. Aizpurua, Phys. Rev. Lett. **105**, 067404 (2010).

[30] N. Sköld, A. Boyer de la Giroday, A. J. Bennett, I. Farrer, D. A. Ritchie, and A. J. Shields, Phys. Rev. Lett. **110**, 016804 (2013).

[31] J. Vučković, ArXiv:1402.2541 [Quant-Ph] **1402.2541**, (2014).

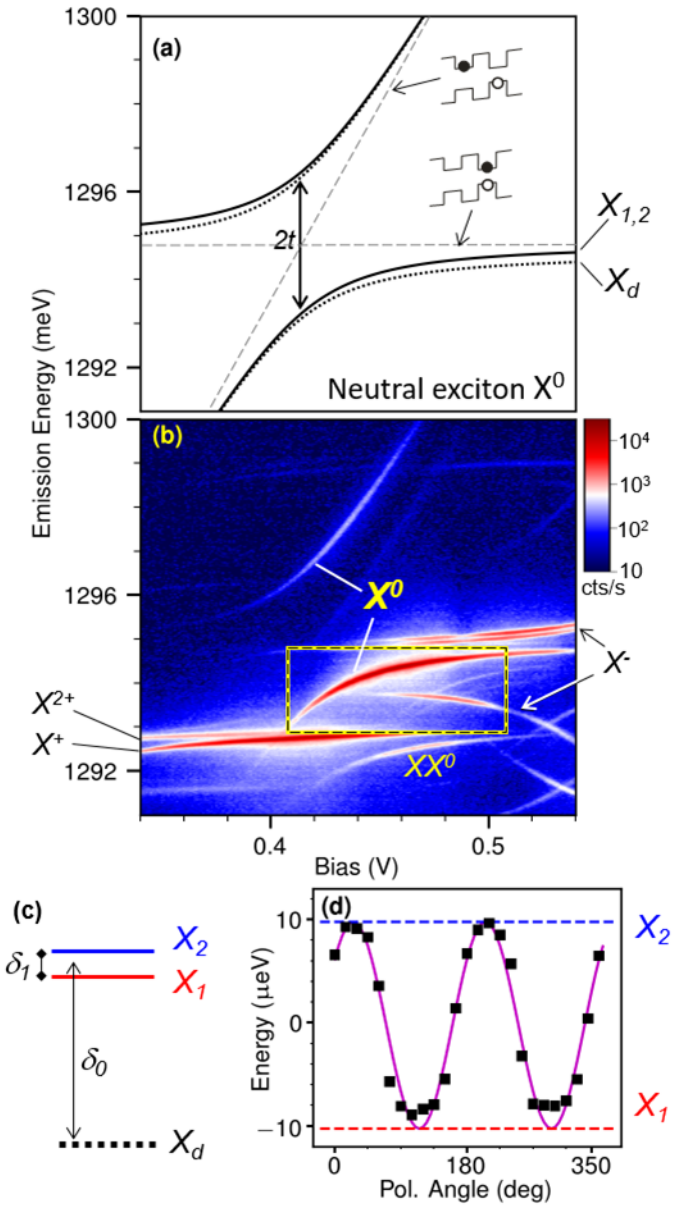

Figure 1 (a) Calculated bias-dependent transition energies of an exciton in a QDM. The anticrossing curves are the eigenenergies, created by a tunneling-induced mixture of direct and indirect excitons (dotted gray lines). The magnitude of the anticrossing is twice the rate (*t)* of a single electron tunneling between the QDs (b) Measured bias-dependent PL spectrum of the neutral exciton X^0. The yellow box indicates the lower branch of the X^0 anticrossing studied in this work and corresponds to the same region shown in Fig. 2. Several other spectral lines correspond to charged excitons that are not studied in this work. X^-, X^+, X^{2+}, XX^0 are labelled here for clarity and further detail is given in [19]. (c) Energy level diagram of the neutral exciton X^0 (not to scale) showing the anisotropic exchange fine structure splitting δ_1 and dark-bright splitting δ_0. (d) Polarization-dependence of exciton PL intensity at 0.515 V. The fine structure splitting δ_1 is obtained from the extrema and the state orientation from the phase (24°).

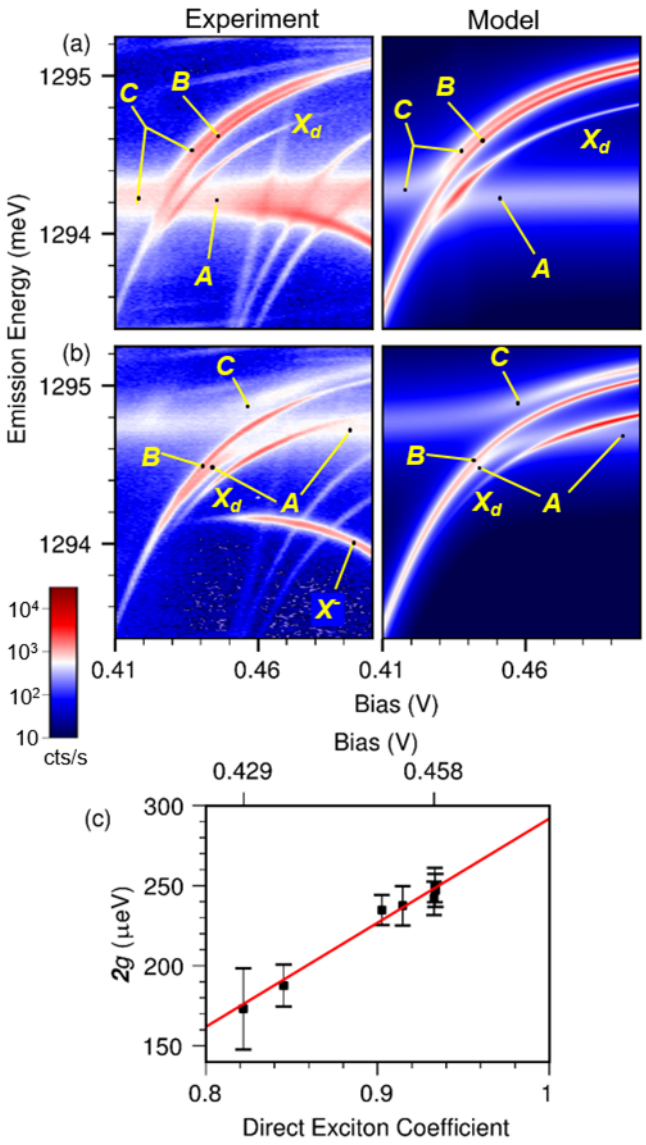

Figure 2 PL spectrum of neutral exciton X^0 versus bias with the cavity resonance tuned to (a) 1294.27 and (b) 1294.77 meV. Measured spectra are in the left column and the results of modelling are on the right. Transition linewidths are phenomenologically accounted for by a complex term in the state energy [31]. In the region of the anticrossing, peaks *A* and *C* are cavity polaritons, while peak *B* is a cavity-induced hybrid of X_1 and X_2. Integrated intensities of each component were normalized for visual clarity. Lines in the experimental data that do not appear in the simulations correspond to charged excitons and are not studied in this work (c) Coupling strength *2g* as a function of direct exciton coefficient (and applied bias).

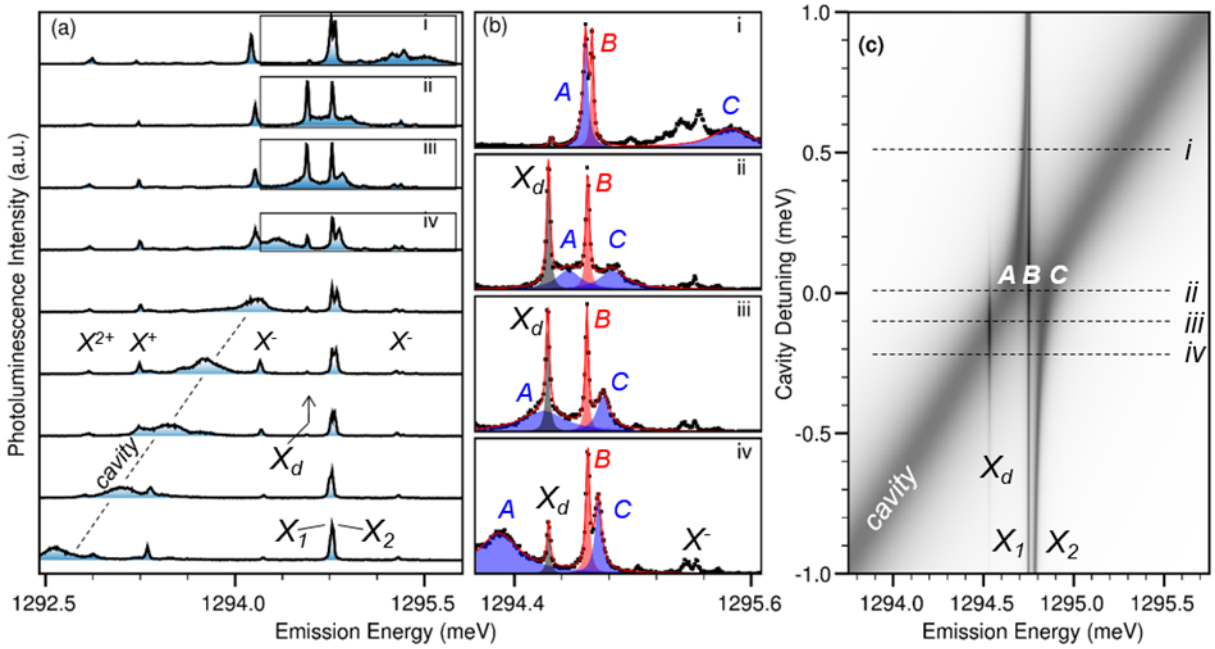

Figure 3 (a) PL spectra of the cavity-QDM system at different cavity-exciton detunings with the bias fixed at ~0.460 V. (b) PL spectra from the boxes i-iv in (a). The red lines are fits to the sum of four Lorentzian functions. Blue, red, and black fills denote fit components for polaritons *A* and *C*, dark exciton X_d, and exciton hybrid state *B*. (c) Modelled spectrum in which peak intensities of each component are normalized for visual clarity. Fits do not include charged exciton peaks such as X^- that are not relevant to the present work.

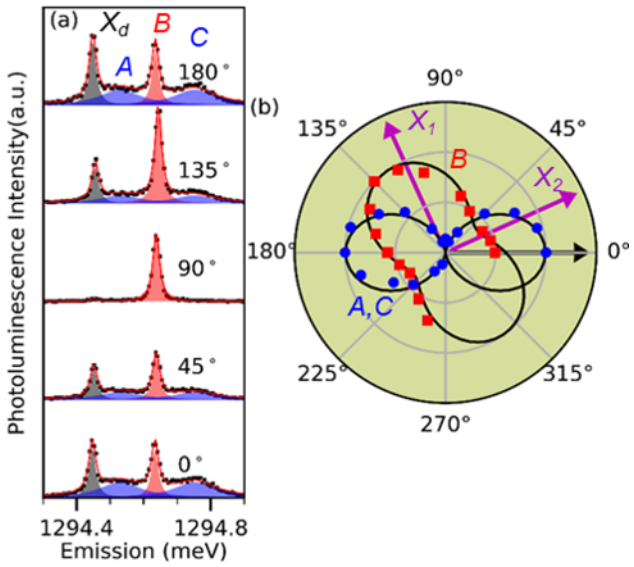

Figure 4 (a) Polarization-dependent PL of the strongly-coupled cavity-QDM system with the cavity tuned to resonance. Peaks *A*, *C*, and X_d are co-polarized with the cavity while *B* has elliptical polarization. (b) Polar diagram of the normalized intensity of peaks *A* and *C* (blue circles) and *B* (red squares) versus analyzer angle. The fits (black) are based on Eq. 1, using the wavefunction coefficients obtained by diagonalizing the model Hamiltonian (see [19]). The orientation of the fine structure states X_1 and X_2 with the cavity resonance detuned are shown by the purple arrows, while the cavity polarization is indicated by the black arrow at 0°.